



Electro-Fenton method for the removal of Malachite Green: effect of operational parameters

Maryam Teymori¹ · Hassan Khorsandi¹ · Ali Ahmad Aghapour¹ · Seyed Javad Jafari¹ · Ramin Maleki²

Received: 4 May 2019 / Accepted: 13 December 2019 / Published online: 24 December 2019
© The Author(s) 2019

Abstract

This study aims to evaluate the degradation and mineralization of Malachite Green (MG) in an electro-Fenton process (EFP). We studied the influence of several important parameters including solution pH (2–11), current density (0–20 mA/cm²), H₂O₂ concentration (0–200 mg/L) and MG concentrations (200, 600, 1000, 1500, 2000, 3000 mg/L) at different reaction time (2.5–30 min). The intermediates produced during the degradation were determined by GC–MS. The optimum pH, current density and H₂O₂ concentration were found to be approximately 3, 10 mA/cm² and 50 mg/L, respectively. It was concluded that acidic pH was required to increase the efficiency of the EFP. At optimum conditions and a reaction time of 15 min, MG was completely removed without any significant variation in the corresponding maximum wavelengths or new absorption bands. Due to formation of intermediates, almost all the organic compounds were completely mineralized (95.3%) to CO₂ and water at reaction time of 30 min. Results indicated the effect of hydroxyl radical (·OH) on MG degradation is greater than that of superoxide radical scavenger (O₂⁻). The results showed that the degradation process of MG followed pseudo-first-order kinetic model and the treatment time required in EFP was 4.6 times lower than ECP. Furthermore, the results showed that EFP was an extremely efficient process for degradation and mineralization of a high concentration of MG (1000 mg/L) at a short reaction time (30 min).

Keywords Advanced oxidation process · Degradation · Electro-Fenton · Malachite Green

Introduction

Synthetic dyes are widely used by several industries such as paper production, textile, leather and food technology. Disposing them to the natural waters can cause serious environmental problems such as decreasing the water transparency and decreasing photosynthesis (Forgiarini and de Souza 2007). On the basis of dye chemical structure, they are classified into various groups such as basic, acidic, azo, diazo and anthraquinone dyes. Currently, 10,000 registered different types of dyes are used in industrials (Ghaly et al. 2014). It is estimated that, this industries spend a lot of water

(approximately 0.08–0.15 m³) to produce 1 kg of fabrics and create up to 1000–2000 m³/d wastewater (Arslan-Alaton et al. 2009; Ghaly et al. 2014). Malachite Green (MG) dye has molecular formula C₂₃H₂₅N₂Cl, and it contains three groups of aryls (molecular weight = 364.92, solubility in water 66.67 g/L as the chloride salt, λ_{max} = 617 nm) (Fig. 1). The MG, a cationic triphenylmethane and also called basic green 4, is extensively used for dyeing cotton, silk, paper, leather and plastics, in acrylic industries and also as biocide in the aquacultural industry due to its high effectiveness as a strong antifungal, antibacterial and antiparasitic agent (Srivastava et al. 2004). Malachite Green is classified as Class II health hazard because it was found to be environmentally persistent and acutely detrimental effects on immune and reproductive system, liver, gill, kidney, intestine, gonads and pituitary gonadotrophic cells (Srivastava et al. 2004; Stolker et al. 2007). Although, Malachite Green has been banned in many countries for aquacultural use, it is still being used due to its low cost, ready availability and efficacy (Li et al. 2012b). Therefore, the removal of MG from aqueous solution is environmentally important.

✉ Seyed Javad Jafari
sjavadj@gmail.com

¹ Department of Environmental Health Engineering, School of Public Health, Urmia University of Medical Sciences, Urmia, Iran

² Research Department of Chromatography, Iranian Academic Center for Education Culture and Research (ACECR), Urmia, Iran

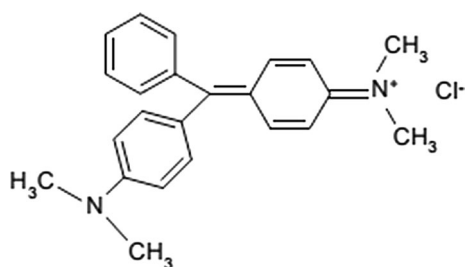
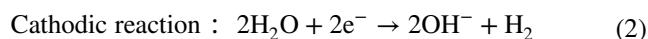
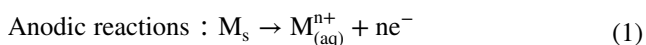


Fig. 1 Structural formula of Malachite Green dye

In recent years, advanced oxidation process (AOP) has been successfully employed as an efficient procedure for degrading organic compounds in aqueous solutions (Hoffmann et al. 1995). In AOPs, the hydroxyl radicals ($\cdot\text{OH}$) are very promising because of their high oxidation efficiency, rapid mineralization and their non-selective reactivity (Hoffmann et al. 1995). Recently, electrochemical AOPs (EAOPs) have received great attention because they are environmentally clean and can produce a large amount of hydroxyl radicals under control of applied current (Peralta-Hernández et al. 2006). Anodic oxidation (AO), so-called direct electrochemical oxidation, and electro-Fenton process (EFP) are the most common EAOPs that are able to produce hydroxyl radical ($\cdot\text{OH}$) for destroying organic pollutants. They are characterized by high standard redox potential ($E = 2.80 \text{ V/SHE}$) (Sirés et al. 2014). Direct electro-oxidation is theoretically possible at low potentials but has slow reaction rate and low $\cdot\text{OH}$ concentration at the anode. Moreover, due to the formation of a polymer layer on the anode surface, there is a decrease in the catalytic activity, commonly called the poisoning effect (Canizares et al. 2004; Rodrigo et al. 2001). In the electro-Fenton process (EFP), by using the coupling of electrochemistry and Fenton's reaction, one of the EAOPs is employed to react with the pollutants. Ting et al. (2008) classified the EF process into four categories. Type 1: sacrificial iron anode is used as a ferrous ion source, while hydrogen peroxide is externally added. Type 2: ferrous ion is externally applied, and hydrogen peroxide is generated by an oxygen-sparging cathode. Type 3: hydrogen peroxide and ferrous ion are electro-generated using an oxygen-sparging cathode and a sacrificial anode. Type 4: Fenton's reagent (Fe^{2+} , H_2O_2) is added to produce hydroxyl radicals in the electrolytic cell, and ferrous ion is regenerated via the reduction of ferric ion on the cathode (Ting et al. 2008). Electro-coagulation process (ECP) includes the generation of coagulants in situ by dissolving electrically iron ions in iron electrodes. The basic reactions that occur in an EC cell are described in the following reactions (Dia et al. 2017):



Most of the researchers used the electro-Fenton technology for the treatment of effluents from the dyeing industry with low concentration. Fe^{2+} was in situ generated at the iron anodes, and hydrogen peroxide was added externally. In this paper, we evaluate the effect of different key variables involved in the EFP, including pH value, current density, H_2O_2 doses, kinetic of the reaction and the presence of different scavengers.

Materials and methods

Chemicals analytical procedures

Malachite Green was purchased from Sigma–Aldrich which was in the crystalline form with purity of 65%. Other chemicals including NaCl , H_2SO_4 and NaOH were analytical grade from Merck. The pH of the solution was adjusted to the desired value at the initial reaction, by adding dilute 0.1 M HCl or 0.1 M NaOH , and was measured by pH meter (Philips PW 9422). The pH of the solution was not controlled during the reaction. Malachite Green was used without further purification in distilled water, using 0.008 M NaCl as supporting electrolyte. This adjustment has shown negligible effect on the initial pH of the solution. At the end of EFP, the residual H_2O_2 in the filtrate was quenched immediately with 5 mM sodium thiosulfate ($\text{Na}_2\text{S}_2\text{O}_3 \cdot 5\text{H}_2\text{O}$). Before analysis, the withdrawn sample was filtered through 0.45 μm acetate cellulose filter, and then, residual dye concentration was analyzed. The removal of color was followed by measuring the drop in absorbance at the maximum wavelength of the dye ($\lambda_{\text{max}} = 617 \text{ nm}$), using a spectrophotometer (Hach, Germany). The removal efficiency was calculated as follows:

$$R(\%) = \frac{C_0 - C_e}{C_0} \times 100 \quad (4)$$

where C_0 and C_e are dye concentrations at the initiation and the end of reaction, respectively. The degree of dye mineralization was measured before and after the processes by determining the total organic carbon (TOC) of the solution using a TOC analyzer (Shimadzu). The mineralization efficiency was calculated as follows:

$$\text{Mineralization efficiency}(\%) = \frac{\text{TOC}_0 - \text{TOC}_t}{\text{TOC}_0} \times 100 \quad (5)$$

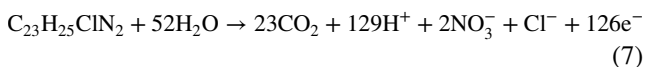
where TOC_0 and TOC_t denote the TOC concentrations before and after oxidation, respectively. Residual H_2O_2

concentration was determined spectrophotometrically (410 nm) using titanium(IV) oxysulfate in accordance with the DIN 38402H15 method (Giannakis et al. 2017).

The concentrations of residual Fe²⁺ and Fe³⁺ ions at the end of electrolysis were determined using the phenanthroline colorimetric method recommended by the American Public Health Association (APHA 1998). The mineralization current efficiency (MCE) of each tested solution was calculated as follows (Guinea et al. 2010):

$$MCE(\%) = \frac{nFV_s \Delta(TOC)_{exp}}{4.32 \times 10^7 mIt} \tag{6}$$

where *F* is the Faraday constant (96,487 C/mol), *V_s* is the solution volume (dm³), Δ(TOC)_{exp} is the experimental TOC decay (mg/dm³), 4.32 × 10⁷ is the conversion factor of units (3600 s/h × 12,000 mg of C/mol), *m* is the number of carbon atoms of MG, *I* is the applied current (A), *t* is the electrolysis time (*h*) and *n* is the number of electrons consumed in the mineralization process of each MG molecule. The *n*-value was taken as 126, considering that each MG is completely mineralized to CO₂ by the reaction (Hashemian 2013):



Experimental setup

A schematic diagram of the experimental setup is shown in Fig. 2. Experimental studies were carried out in an undivided electrochemical cell with a volume of 250 mL by constant agitation with a magnetic stirrer at a rate of 300 rpm.

Cylindrical glass vessel made from Pyrex having 5 cm internal diameter and a 25 cm height operated in the batch mode. Electrochemical cell was equipped with a cathode and an anode, both made of iron and installed in parallel. Initial experiments were conducted at room temperature of 25 °C. In order to do electrolyses, the electrodes were connected to a digital DC power supply (GW Instek, GPS 3030 DD, 0–30.0 V, 0.0–5.0 A). Simultaneously, a certain amount of H₂O₂ was added into the solution, current density was adjusted to the desired value and the electrolysis was started. The area of both electrodes plunged into the beaker containing dye solution had a length × width × thickness dimension of 4 cm × 2.5 cm × 0.2 cm. Two sheets of iron spaced 1 cm apart were installed in the cell’s electrodes

All the chemical analyses were carried out according to the detailed procedure in standard methods for examination of water and wastewater (APHA 1998). In this study, EFP trials were conducted for different pH values (2, 3, 5, 7, 9, 11), current densities (0, 2.5, 5, 7.5, 10, 15, 20 mA/cm²), H₂O₂ doses (0, 25, 50, 75, 100, 150, 200 mg/L) and MG concentrations (200, 600, 1000, 1500, 2000, 3000 mg/L) at different reaction time (2.5–30 min) (kinetic of reactions). The EFP of MG was repeated by adding 3 mM of (SO₄²⁻, PO₄³⁻) as an anion, 3 mM of EDTA as a hole (h⁺) scavenger and chelating agent, 3 mM of benzoquinone (BQ) as a superoxide radical scavenger (O₂⁻) and 10 mM of tert-butyl alcohol (TBA) as a hydroxyl radical scavenger (·OH) (Xin et al. 2016). Also, in the optimum condition of the experiment the intermediates produced during the degradation were determined by GC–MS. The operation phases and experimental conditions are given in Table 1. Experimental studies independently were repeated twice, and data are presented as

Fig. 2 The experimental setup

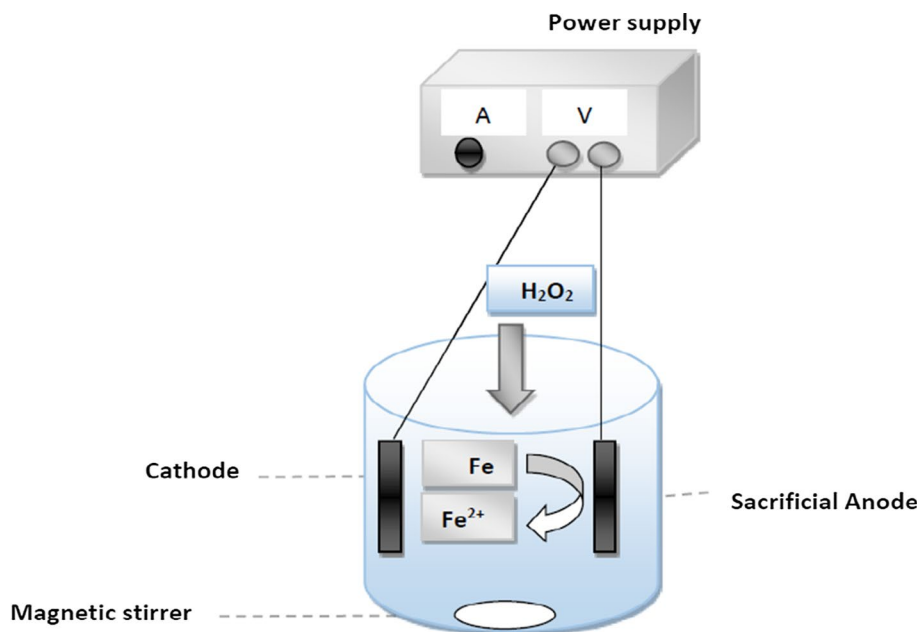


Table 1 The operation phases and experimental conditions

Operation phase	pH	CD (mA/cm ²)	MG concentration (mg/L)	H ₂ O ₂ doses (mg/L)	Time reaction (min)	Scavengers/chelating agent
Effect of pH	2–11	7.5	200	50	10	No ingredient
Effect of CD	Inherent (pH=3)	0–20	200	50	10	No ingredient
Effect of H ₂ O ₂ doses	Inherent (pH=3)	10	200	0–200	10	No ingredient
Time reaction (min) and MG concentration (kinetic study)	Inherent (pH=3)	10	200–3000	50	2.5–30	No ingredient
Effect of scavengers	Inherent (pH=3)	10	200	50	15	(SO ₄ ²⁻ , PO ₄ ³⁻ , tert – butyl, EDA)

mean \pm standard deviation (SD). In addition, the efficacy of the ECP in the removal of MG was also evaluated. In ECP, the addition of H₂O₂ was stopped to the reactor while the power supply was kept switched on. In addition, characteristic of the waste sludge produced from the method was also observed. Sludge production was determined by TSS (total suspended solids) and SVI (sludge volume index) according to Standard Methods (APHA 1998).

Analysis of metabolites formed after decolorization

Extraction of degradation metabolites

A 50.0 mL of sample solution was transferred into a volumetric flask, and then 1 mL of n-hexan was added and vigorously stirred for 10 min. After separation of organic phase from water sample, the organic phase was transferred to an Eppendorf microtube containing 100 mg anhydrous Na₂SO₄ and mixed well for 5 min. The mixture was centrifuged at 5000 rpm for 3 min. A 500 μ L portion of organic phase was transferred into a 1.0 mL vial, and 1 μ L was injected into the GC–MS (Cui et al. 2016; Wanyonyi et al. 2017).

GC–MS Analysis

Malachite Green degradation metabolites analysis was performed on an Agilent 7890 gas chromatograph equipped with an Agilent 5975C mass spectrometer detector, equipped with HP-5MS capillary column (30 m \times 0.25 mm i.d., 0.25 μ m film thicknesses) and ChemStation software. Helium was used as carrier gas with the flow rates of 1 mL/min. The initial temperature of column was maintained at 50 °C for 1 min and then raised at 5 °C/min to 180 °C and held for 2 min and then raised at 10 °C/min to 260 °C and held for 15 min. Injection of samples was carried out in splitless mode. The injector, detector, line transfer and ion resource temperatures were set at 250 °C, 260 °C, 280 °C and 230 °C, respectively (Cui et al. 2016; Wanyonyi et al.

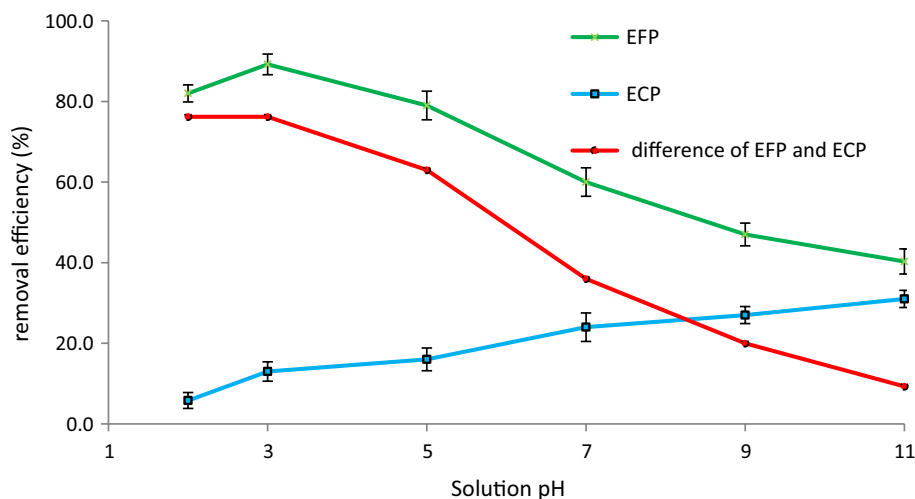
2017). Mass spectra were scanned in the range of 40–500 amu. Identification of individual compounds was made by comparison of their mass spectra with those of the internal reference Wiley 7NL mass spectra library.

Results and discussion

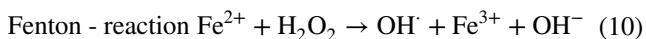
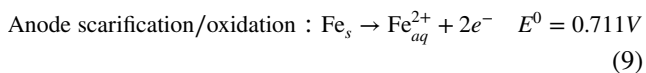
Effect of pH and the mechanism MG degradation

The effect of pH at different pH values (2, 3, 5, 7, 9, 11) on the degradation of MG in the ECP and EFP was investigated under the conditions specified in Table 1. The degradation of MG as a function of pH is shown in Fig. 3. As observed in Fig. 3, the highest electro-Fenton activity was attained under pH 3, where the MG removal reached near 89%. These findings confirm that EFP and ECP efficiency is a function of pH. Based on the results plotted in Fig. 3, the removal of MG in EFP increased from 82% at pH 2 to 89.2% when pH was increased to 3. A further increase in pH to 11 led to a considerable decline of MG removal to 40.3% under the selected conditions. This result is entirely consistent with the findings of other authors which indicated that the optimal pH of Fenton process is around 3 (Guenfoud et al. 2014; Hameed and Lee 2009; Hashemian 2013; Panizza and Cerisola 2009b; Wang et al. 2010). For instance, Hameed and Lee (2009) investigated the degradation of Malachite Green by Fenton process and observed the maximum degradation of MG in a [dye] = 20 mg/L, [H₂O₂] = 20 mM and [Fe²⁺] = 0.05 mM at pH level 3. Similarly, Panizza and Cerisola (2009b) reported that electro-Fenton process reached its maximum degradation of Alizarin Red at pH 3.0 with a maximum COD removal of 93% at 4 h. At low pH values below 3, hydrogen peroxide would stay steady according to the formation of oxonium ion as shown in Eq. 8. Furthermore, iron species form stable complexes (e.g., Fe(H₂O)₆²⁺) with H₂O₂ at lower pH values, leading to deactivation of catalysts (Zhou et al. 2007):

Fig. 3 Effect of solution pH on MG degradation in EFP and ECP (initial MG concentration = 200 mg/L; current density = 7.5 mA/cm²; H₂O₂ dosage = 50 mg/L; reaction time = 10 min)



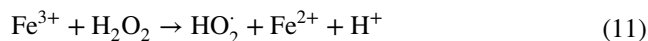
On the other hand, iron species began to precipitate as ferric hydroxides (Fe(OH)_n) at higher pH values and thus the ratio of Fe²⁺/Fe³⁺ decreased (Jiang and Zhang 2007). In this way, when the solution pH further increased oxidation together with simultaneous coagulation and formation of hydroxyl complexes, these ferric hydroxide complexes led to the deactivation of a ferrous catalyst (Szpyrkowicz et al. 2001). Thus, due to the EFP result of co-action of hydrogen peroxide and ferrous ion, the conversion of Fe²⁺ and Fe³⁺ to Fe(OH)_n-type structures led to the degradation tendency of MG at different pH values (Zhou et al. 2007). Moreover, H₂O₂ rapidly decomposed to oxygen and water at basic solution with rate constant of 2.3 × 10⁻² and 7.4 × 10⁻² min⁻¹ at pH 7.0 and 10.5, respectively (Shemer and Linden 2006). The maximum percentage removal of EFP in removal of MG attained at pH = 3 can be stated considering the continuous release of Fe²⁺ through anodic scarification/oxidation [Eq. (9)] and the classic Fenton reaction [Eq. (10)] (Eiroa et al. 2005):



Therefore, according to Fig. 3 maximum difference of EFP and ECP efficiency in removal of MG was observed at an acidic pH. It was concluded that acidic pH was required to increase the efficiency of the EFP. This narrow pH range for the EF process limits the perfect application of this technology in wastewater treatment. Hopefully, inherent pH of MG is 3 and there is no need to adjust pH. Ray et al. (2006) reported that pH of wastewater outputs from acrylic fiber industry (its wastewater contains MG) at low pollution load is 4. Li et al. (2012a) reported that Fenton process reached

its maximum degradation of acrylic fiber manufacturing wastewater at pH 3.

However, the Fe³⁺ formed during Eq. (10) cause one of the parasitic reactions in EFP. According to Eq. (11), Fe³⁺ by consumption of H₂O₂ and thus competing with the main Fenton reaction can cause limiting generation of ·OH (Eiroa et al. 2005):

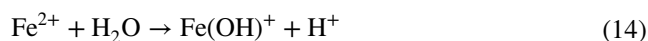


The MG was degraded through the generated reactive radicals (hydroxyl and hydroperoxyl) (Eq. 12 and Eq. 13):



As the oxidation potential of ·OH (2.8 eV) is much higher than that of HO₂· (E° = 1.65 V), in the presence of HO₂· the contribution of reaction (12) in degradation of MG was more decreased than that of reaction (13). Therefore, the occurrence of a parasitic reaction [Eq. (11)] led to limiting the rate of MG degradation (Eiroa et al. 2005).

Based on the results plotted in Fig. 3, the removal of MG in ECP (reaction without H₂O₂) increased from 5.8% at pH 2 to 31% when pH was increased to 11. According to the speciation curve of Fe(II) in water [Eq. (14)], Fe(OH)⁺ is the dominant species of iron in the solution with a strong alkaline pH (over 9). The increase in pH during ECP process leads to coagulation of MG and is removed by electrostatic attraction (Santana-Casiano et al. 2006):



In aqueous solution, MG exists in two ionic forms: cationic form and colorless carbinol form (Mitrowska et al. 2008). The carbinol base is colorless and relatively insoluble in

water. MG has two amino groups with pKa of 6.9 that are complete protonated and ionized at pH 4 or lower. At pH 10, most molecules are deprotonated, exist solely as the carbinol and so colorless (Mitrowska et al. 2008).

Effect of current density

To choose the suitable applied current density for optimal MG removal in the EFP and ECP, several experiments at an applied current density ranged from 0 to 20 mA/cm² were investigated (under the conditions given in Table 1). Figure 4 shows the results of MG removal as a function of current density. Figure 5 shows the H₂O₂ consumption percentage versus the current density at a constant H₂O₂ concentration of 50 mg/L.

As shown in Fig. 4, when no current was applied between the electrodes, 9% of MG was removed. This can

be attributed to Fenton reaction in the cell between the Fe electrodes and the H₂O₂ added to the reactor. Consumption of added H₂O₂ (4%) and the reduction in weight of both electrodes (0.0025 g weight reduction for each electrode) prove this reasoning. As illustrated in Fig. 4, at the low current density of 2.5 mA/cm², 76% of the MG could be removed. The increase in current density to 10 mA/cm² caused an increase in removal of MG to 94%. However, a further increase in current density to 15 mA/cm² had insignificant influence on MG removal. Since the consumption of electric energy increased with the applied current, accordingly the best applied current density of 10 mA/cm² was selected for the electrodes in the next experiments. According to Faraday's formula (Eq. (15)), it is clear that Fe²⁺ dose released from anode depends on the current (Daneshvar et al. 2006):

Fig. 4 Effect of current density on MG degradation in EFP and ECP (initial MG concentration = 200 mg/L; solution pH = inherent (3); H₂O₂ dosage = 50 mg/L; reaction time = 10 min)

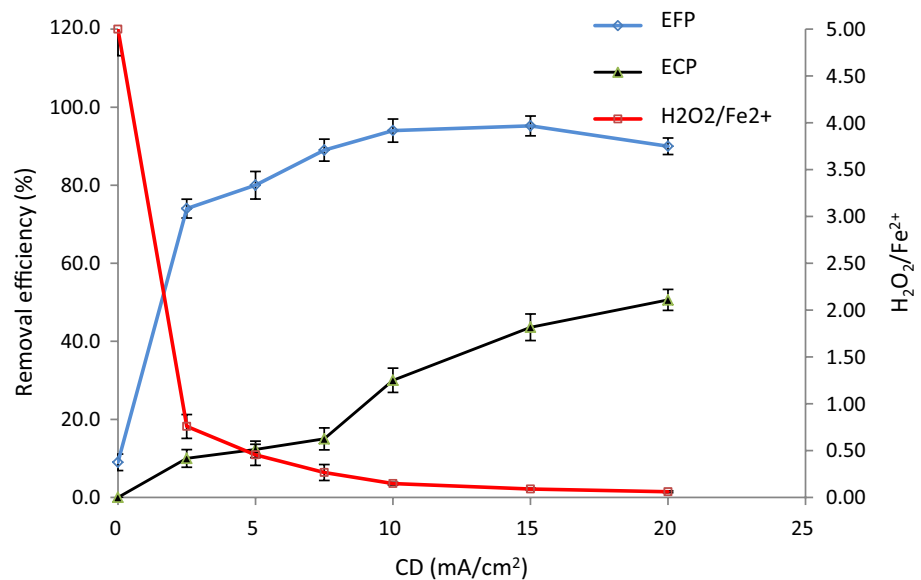
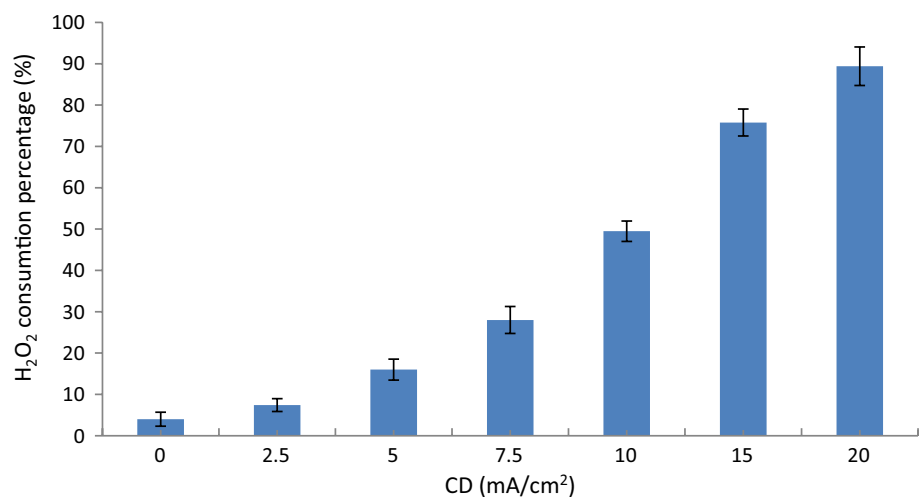


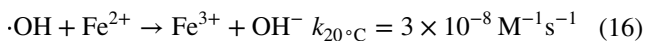
Fig. 5 H₂O₂ consumption percentage versus the current density (initial MG concentration = 200 mg/L; solution pH = inherent (3); H₂O₂ dosage = 50 mg/L; reaction time = 10 min)



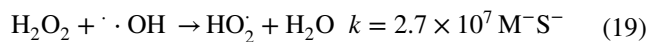
$$C_{Fe} = \frac{M_w It}{ZFV} \tag{15}$$

where C_{Fe} , Z, F, V, M_w and t are the theoretical concentration of Fe^{2+} (g/m^3), the chemical equivalence ($Z_{Fe} = 2$), Faraday constant ($96,487 C equiv^{-1}$), volume of reactor (m^3), molecular weight of iron ($= 56 g/mol$) and electrolysis time (s), respectively.

Applying an electrical current until density of $15 mA/cm^2$ resulted in an increase in MG removal to 95.2%. It appeared that higher current densities, according to Faraday's law, accelerate anodic scarification and the generation of Fe^{2+} ions, which is a main element required to run the Fenton reaction (Moussavi et al. 2011, 2012). Determination of the ratio of mass of H_2O_2 added to the reaction cell to the mass of Fe released to the solution ($H_2O_2/Fe(II)$) verifies this deduction. As shown in Fig. 4, with increasing intensity of current, the ratio of H_2O_2/Fe declines. The increase in weight loss of anode electrode, which according to Eq. (9) means an increase in $Fe(II)$ released to the solution, resulted in the decline of $H_2O_2/Fe(II)$ ratio with increased intensity of current since the total amount of H_2O_2 added to the reactor at all current densities was constant at 50 mg/L. In the presence of greater $Fe(II)$ available in the solution, reaction of EFP [Eq. (10)] accelerated. Therefore, a greater amount of H_2O_2 consumption (Fig. 5) and hence a higher amount of $\cdot OH$ were generated which resulted in an increase in MG removal. A significant amount of flocs were generated, when the current density increased which in turn trapped the dye molecules and enhanced the EFP efficiency (Fig. 4) (Khattee et al. 2009). As shown in Fig. 4, a further increase in current density to $20 mA/cm^2$ decreased MG removal to 90%. At current densities of over $15 mA/cm^2$, the decline in MG removal in EFP can be related to higher anode scarification and generation of the excess concentration of Fe^{2+} . According to Eq. (16), the excess Fe^{2+} scavenged the $\cdot OH$ and so decreased the $\cdot OH$ available to react with MG (Pérez et al. 2002):



Moreover, at higher current density, competitive electrode reaction and parasitic reaction will increase (Nidheesh and Gandhimathi 2012). These reactions include equations of (17), (18) (19) and (20) (Nidheesh and Gandhimathi 2012). The reaction rate constant (k) of Eqs. (19) and (20) is more than 500,000 times greater than k reaction of Eq. (10) (Moussavi and Aghanejad 2014; Nidheesh and Gandhimathi 2012). These reactions inhibit main reactions such as reactions (10) which cause a decrease in efficiency of EFP:



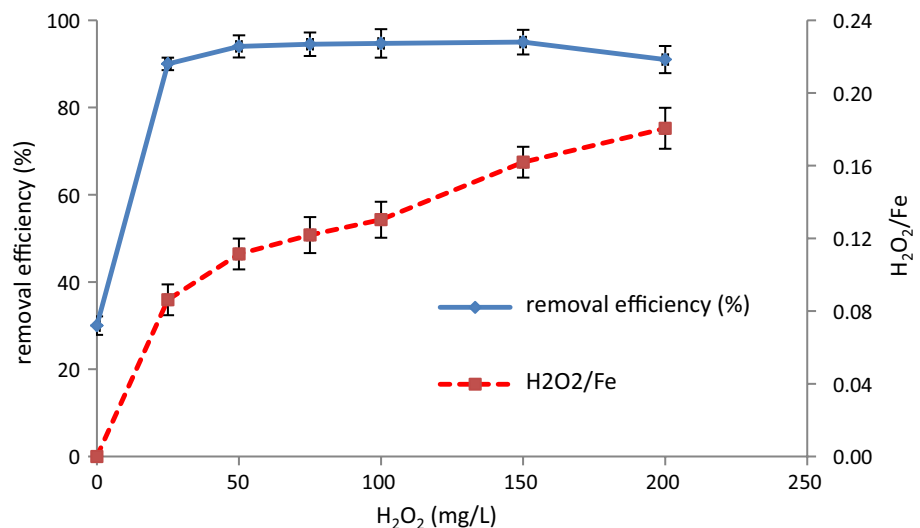
As shown in Fig. 4, MG removal in the ECP at the current density of 2.5, 5, 7.5, 10, 15 and $20 mA/cm^2$ was 10%, 12.3%, 15%, 30%, 43% and 50.6%, respectively. On the other hand, in the presence of NaCl, oxidant species can be generated by the indirect electrochemical oxidation (Garcia-Segura et al. 2018). In order to determine the role of indirect electrochemical oxidation, the effect of current density for ECP without NaCl was done. Results showed that MG degradation in the ECP without NaCl at the current density of 2.5, 5, 7.5, 10, 15 and $20 mA/cm^2$ was 9%, 11.5%, 14.3%, 29%, 43% and 50%, respectively. It can be seen in the absence of NaCl removal efficiency of MG at ECP negligible decreased. Therefore, role of indirect electrochemical oxidation at degradation of MG is insignificant. This finding agrees with reported in the literature (Ghoneim et al. 2011) which determined that in the presence of Cl^- ions the efficiency of electrochemical oxidations is lowered, whereas in the presence of other supporting electrolyte.

Effect of H_2O_2 dosage

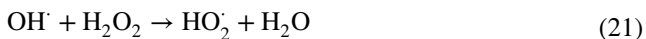
The initial concentration of H_2O_2 plays an important role in the EFP (Ting et al. 2009). The effect of H_2O_2 dosage on degradation of 200 mg/L MG was investigated at current density of $10 mA/cm^2$, pH of inherent and time reaction of 10 min. The ratio of mass of H_2O_2 to that of Fe^{2+} was calculated from the H_2O_2 added to the reactor cell and the Fe^{2+} released by Fe anode scarification. Therefore, the H_2O_2 concentrations as a function of the percentages of MG removal and the molar ratio of H_2O_2 to Fe^{2+} are shown in Fig. 6. As shown in Fig. 6, in the absence of H_2O_2 , the rate of MG removal was only 30% (electro-coagulation). Doses of 25, 50, 75, 100 and 150 mg/L H_2O_2 resulted in an increase in MG removal to 90, 94, 94.5 94.7 and 95%, respectively. The increase in removal of MG with an increased dose of H_2O_2 was due to the increase in hydroxyl radical concentration as a result of the addition of H_2O_2 [Eq. (10)]. In this way, the optimum ratio of H_2O_2 to Fe^{2+} was determined to be approximately 0.11 (mg H_2O_2 to mg Fe^{2+}).

The further increase in H_2O_2 concentration to 200 mg/L caused MG removal efficiency to decrease down to 91%. At a high dosage of H_2O_2 , the decrease in removal efficiency was due to competing parasitic reactions that cause scavenging effect of H_2O_2 (Eqs. (21) and (22)) and the recombination of the hydroxyl radical (Eq. (18)) (Babuponnusami

Fig. 6 Effect of H_2O_2 dosage (0–200 mg/L) on MG degradation in EFP (initial MG concentration = 200 mg/L; solution pH = inherent (3); current density = 10 mA/cm²; reaction time = 10 min)



and Muthukumar 2012; Muruganandham and Swaminathan 2004):



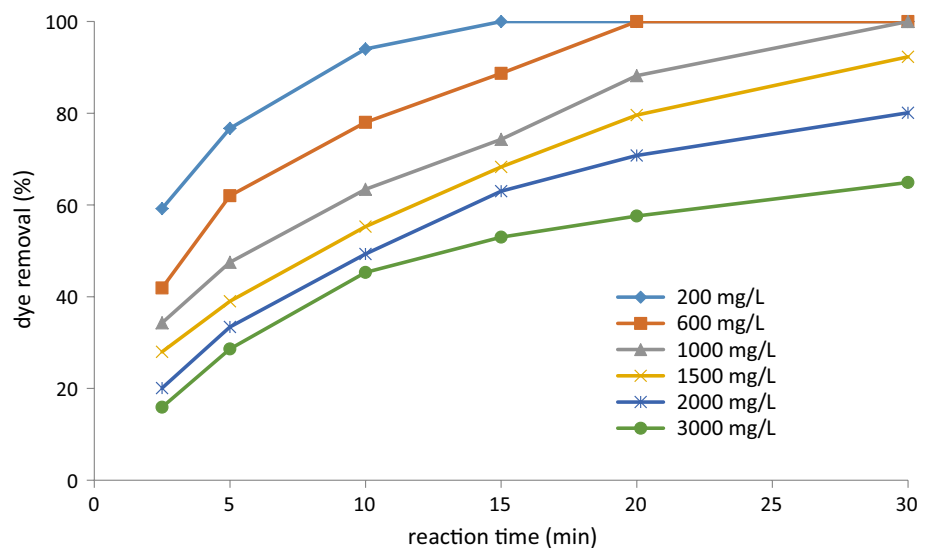
Oxidation potentials of hydroperoxyl radicals are less than H_2O_2 . Oxidation potentials of H_2O_2 and hydroperoxyl radicals are 1.31 and 1.25, respectively, as compared to chlorine: 1.0 (Rodríguez 2003)

Kinetic study of EFP

The effect of MG concentration on its decay kinetic during EFP at 10 mA/cm² and 50 mg/L H_2O_2 is shown in Fig. 7. As anticipated, a longer time of electrolysis was required to

remove MG as its initial concentration increases due to the superior amount of organics in medium (Panizza and Oturan 2011). The results given in Fig. 7 indicated that removal efficiencies of MG dye were decreased with increasing initial concentrations. For instance, at first 15 min, the removal efficiency observed at initial MG concentrations of 200, 600, 1000, 1500, 2000 and 3000 mg/L was 100, 88.7, 74.3, 68.3, 63 and 53%, respectively. Under the constant conditions of the electrolysis system such as the constant current density, a specified amount of hydroxyl free radicals are produced. When the concentration of the pollutant is increased, the amount of hydroxyl free radicals is not enough to degrade the high concentrations of the pollutant, and thus, removal efficiency decreases (Daneshvar et al. 2008). Furthermore, the result showed that EFP at optimum condition could remove 100% of MG at an inlet concentration up to 1000 mg/L and 92.3, 80.1 and 65% at initial MG concentration of 1500, 2000 and 3000 mg/L in short time

Fig. 7 Effect of MG concentration on its degradation (CD = 10 mA/cm², solution pH = inherent (3), $C_{\text{H}_2\text{O}_2} = 50 \text{ mg/L}^{-1}$)



reaction as low as 30 min. Considering the fact that the concentration of most fish industry MG-laden effluents is below 100 ppm, it can be concluded that the EFP is an efficient and promising technique for treating fish industry wastewaters containing dyes compounds (Culp and Beland 1996). On the other hand, in most published literature, the concentration of MG removed was less than 50 mg/L (Gokulakrishnan et al. 2012; Guenfoud et al. 2014).

Pseudo-first- and pseudo-second-order reaction kinetics were used to study color removal kinetics for EFP. The individual expressions were presented as follows [Eqs. (23), (24)]:Pseudo-first-order reaction kinetics:

$$\text{Ln}C_t = \text{Ln}C_0 - K_1 t \tag{23}$$

Pseudo-second-order reaction kinetics:

$$\frac{1}{C_t} = K_2 t + \frac{1}{C_0} \tag{24}$$

Table 2 Kinetic parameters for degradation of MG at different initial concentrations by EFP (CD=10 mA/cm², pH=3, C_{H2O2}=50 mg/L-1)

Malachite Green concentration(mg/L)	Pseudo-first order		Pseudo-second order	
	<i>K_{app}</i>	<i>R</i> ²	<i>K_{app}</i>	<i>R</i> ²
200	0.2578	0.9979	0.0099	0.9548
600	0.1275	0.9956	0.0009	0.9537
1000	0.0927	0.9682	0.0004	0.8418
1500	0.0805	0.9893	0.0003	0.8494
2000	0.0509	0.9874	0.00007	0.9907
3000	0.031	0.9323	0.00002	0.9813

where *C*₀ and *C*_{*t*} show the MG concentration at the beginning and after time (*t*) of the reaction, respectively. *K*₁ and *K*₂ show the pseudo-first- and pseudo-second-order reaction constants, respectively. Values of *K*₁ and *K*₂ can be determined analytically from the slope of the plots Ln *C*_{*t*} against *t* and 1/*C*_{*t*} against *t*, respectively (Moussavi et al. 2011). Table 2 shows the obtained values of *K_{app}* and liner correlation (*R*²) from pseudo-first- and pseudo-second-order kinetics. According to the correlation coefficients (*R*²) given in Table 2, the experimental data fitted better to the pseudo-first-order reaction (higher values of *R*²). Furthermore, according to Table 2, the pseudo-first-order rate constants slightly decreased with increasing the concentration of MG dye which was due to the progressive acceleration of competitive reactions between hydroxyl free radicals and the lately formed oxidant by-products of MG dye during the process (El-Desoky et al. 2010; Hafaiedh and Bellakhal 2013).

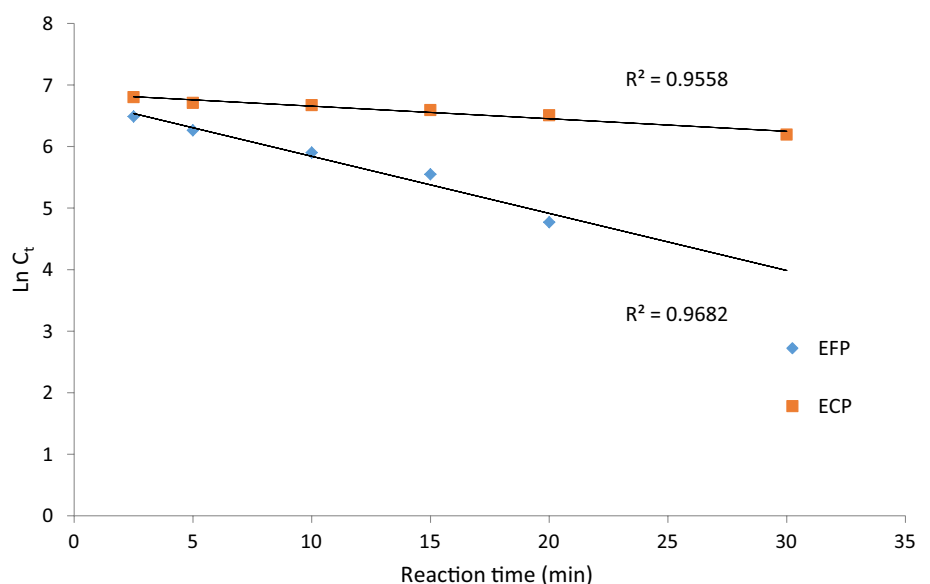
To better determine the rate reaction in EFP and ECP, the kinetics of MG removal with pseudo-first-order reaction is shown in Fig. 8. As shown in Fig. 8, reaction rate constants for EFP and ECP were 0.092 and 0.02 min⁻¹, respectively. Thus, predicting a model for the removal of MG in the EFP and ECP can be proposed as follows:

$$\text{EFP} : r_{\text{MG}} = 0.092(C_t)^2 \tag{25}$$

$$\text{ECP} : r_{\text{MG}} = 0.02(C_t)^2 \tag{26}$$

Accordingly, the treatment time required in EFP is 4.6 times lower than ECP.

Fig. 8 The plots of pseudo-first-order reaction models fitted in EFP and ECP (C_{MG}=1000 mg L⁻¹, C_D=10 mA/cm², pH=3, C_{H2O2}=50 mg L⁻¹)



Characteristic of the waste sludge

One of the most important advantages of EFP in comparison with Fenton process is waste sludge having low amount and high settling properties. To prove this point, TSS and SVI of the waste sludge produced from the EFP and Fenton process in optimum conditions (pH=3, applied current density 10 mA/cm², H₂O₂ concentration 50 mg/L for EFP and 0.3 g/L iron powder depending on the weight loss of the anode electrode in EFP and H₂O₂ concentration 50 mg/L for Fenton process) were determined. The result showed that TSS is 1540 and 2570 mg/L in EFP and Fenton process, respectively. The SVI value for EFP was determined 7 ml/g, while sludge in Fenton process was not deposited. SVI value lower than 100 is considered as the sludge having good sedimentation characteristics (Tchobanoglous et al. 2003). According to Panizza and Oturan (2011), reaction (10) is reproduced through the continuous regeneration of ferrous iron at the cathode (reaction (27)) Accordingly, accumulation of Fe³⁺ and thereby production of iron sludge are eliminated:



Therefore, low amount and high settling properties of EFP in comparison with Fenton process may considerably reduce disposal costs of waste sludge produced for large-scale treatment systems. The standard for effluent discharge regulations for iron is 2 mg/L (EPA. 2002). Results showed at optimum conditions, the residual concentration of iron (Fe²⁺+Fe³⁺) in treated effluent (supernatant) is 5.8 mg/L. So, using the conventional treatments or the electro-Fenton, excess of the metal would be removed.

MG mineralization, UV–Vis spectra and identification of intermediates

To conduct investigation of intermediates, the mineralization of MG was studied by measuring the TOC. The TOC decay with electrolysis time of 200 mg/L MG solution under best conditions, previously found, (pH of inherent, applied current density 10 mA/cm² and H₂O₂ concentration 50 mg/L) is presented in Fig. 9. The results in Fig. 9 show that TOC is reduced by 62.3% for 5 min and by 95.3% for 30 min. This finding means that almost all the organic compounds are completely mineralized to CO₂ and water. Figure 9 depicts the time of MCE values calculated from Eq. (6). As expected, the efficiency was 19.4% at the beginning of the electrolysis and then it gradually decreased during the treatment. This tendency can be related to the gradual formation of more recalcitrant by-products that are more difficult to destroy with electro-Fenton oxidation (Panizza and Cerisola 2009a; Panizza and Oturan 2011). Panizza et al. also reported similar observation (Panizza and Oturan 2011). They investigated the degradation of Alizarin Red by electro-Fenton process using a graphite-felt cathode and observed that TOC removal efficiency and MCE at reaction time of 40 min and 210 min are 25%, 95% and 55%, 30%, respectively.

In order to appear the changes in the molecule of MG and to unfold the mechanism of electro-Fenton degradation, time-dependent UV–Vis spectra of MG solution during EFP were drawn. Figure 10 shows typical time-dependent UV–Vis spectra of MG solution during EFP at current density of 10 mA/cm², initial concentration of 200 mg/L and pH of inherent. As shown in Fig. 10, it could be observed that before treatment, the MG was characterized by a strong band

Fig. 9 TOC removal and mineralization current efficiency (MCE) of MG by EFP (initial MG concentration = 200 mg/L; solution pH = inherent (3); current density = 10 mA/cm²; H₂O₂ dosage = 50 mg/L)

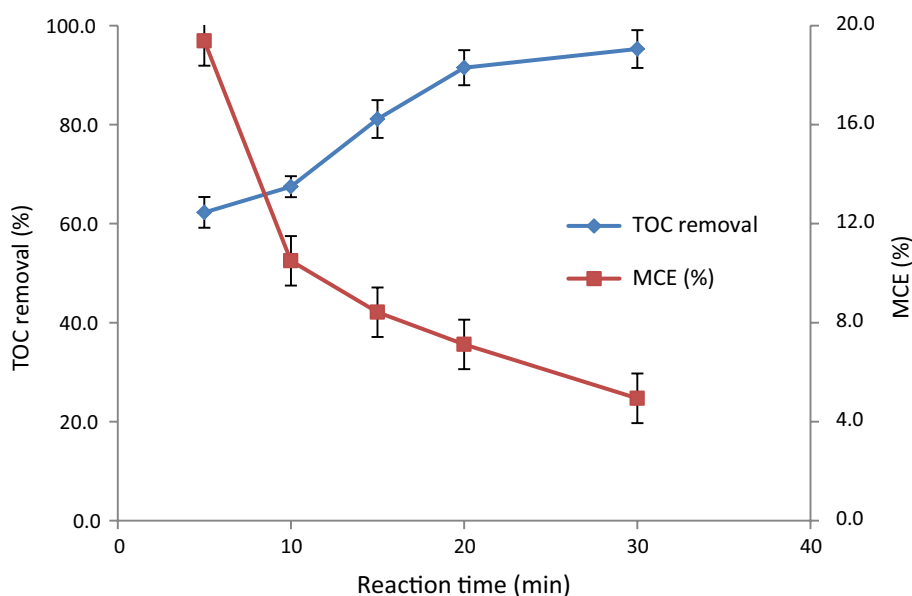
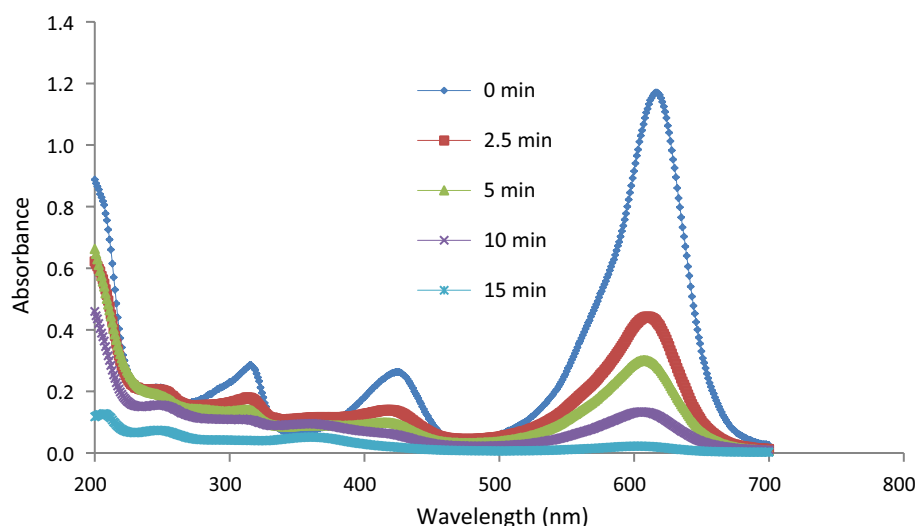


Fig. 10 The absorption spectra of MG degradation at typical time (initial MG concentration = 200 mg/L; solution pH = inherent (3); current density = 10 mA/cm²; H₂O₂ dosage = 50 mg/L)



at the characteristic $\lambda_{\max} = 617$ nm, along with two other weaker bands centered at 425 and 361 nm. Different structural groups in the dye molecules have unique absorbance peak, and these bands correspond to the chromophore group, the benzenic rings and the acidic functionality, respectively (Guenfoud et al. 2014). As it is clear from Fig. 10, the intensity of absorption peaks underwent a gradual decrease with EFP time up to their disappearance and became almost zero at ~ 15 min without any significant variation in the corresponding maximum wavelengths or new absorption bands. This indicates that the MG had been rapidly degraded (Zhou et al. 2007). The sooner decrease in MG concentration, measured by UV–Vis compared to solution TOC removal efficiency, indicates that some intermediates are produced during the oxidation (Panizza and Oturan 2011).

The intermediates formed during the degradation were determined by GC–MS as shown in Table 3. As can be seen, the most important intermediates included aromatic compounds (1,2-Benzenedicarboxylic acid, Benzene, 1,2-Benzenedicarboxylic acid) and benzoic acid (with 54.3% peak

area). Therefore, the first stage of decomposition of the dye MG molecule occurs from cleavage of the bond between the central carbon, by attack of $\cdot\text{OH}$, leading to the production of aromatic compounds (Oturan et al. 2008; Xie et al. 2001). Benzoic acid and methyl ester generated after splitting of the bond between the central carbon of MG and phenylic groups. Eventually, this ultimate intermediate can be finally converted to CO₂. Oturan et al. (2008) reported that the degradation of Malachite Green by Fe³⁺-catalyzed electro-Fenton process yielded aromatics including phenols, benzophenones and benzoic acid derivatives, which were converted into hydroquinone and p-benzoquinone. The cleavage of these products led to aliphatic carboxylic acids.

Effect of scavengers

In order to confirm the mechanism of oxidation of organic compounds in the EFP occurred through hydroxyl radicals and electro-Fenton reaction, several experiments were run with EFP in the presence of various well-known radical

Table 3 Metabolites of Malachite Green degradation analyzed by GC–MS

No.	Compound name	Molecular weight (g/mol)	$t_{R(\text{min})}$ (min)	Peak area (%)
1	1,2-Benzenedicarboxylic acid	166.131	22.975	1.750
2	p-Benzylaminophenol	197.230	25.167	3.647
3	Benzene,1-dimethylamino-4 phenyl	163.220	25.287	1.375
4	Aminoacetic acid	24.990	25.893	11.014
5	1,2-Benzenedicarboxylic acid, butyl ester	212.130	26.506	6.573
6	m-(Dimethylamino)benzoic acid	165.190	26.952	5.635
7	1,4-Naphthalenedione	158.153	27.272	2.167
8	4-Nitrobenzophenone	227.210	28.674	13.508
9	Benzoic acid, methyl ester	136.150	28.909	54.332

Retention time (t_R)

inhibitors/scavengers including (SO_4^{2-} , PO_4^{3-}) as an anion, EDTA as a hole (h^+) scavenger and chelating agent, benzoquinone (BQ) as a superoxide radical scavenger (O_2^-) and tert-butyl alcohol (TBA) as a hydroxyl radical scavenger ($\cdot OH$) at the optimum current density of 10 mA/cm², pH of inherent (= 3) and a constant reaction time of 15 min. The result showed that the efficacy of EFP in the absence of radical scavengers was 100% under the selected conditions. When EDTA, phosphate, TBA, sulfate and BQ were added to the dye solution, the degradation of MG dropped dramatically to 60%, 70%, 81%, 85% and 94%, respectively. The most reduction effect was obtained by EDTA (40% reduction effect). Since EDTA is a strong chelating agent with a high reaction rate constant with Fe^{2+} , subsequently it causes a reduction in $\cdot OH$ production and thus a decrease in MG degradation. The presence of EDTA, as deduced above, confirms the generation of $\cdot OH$ in the EFP (Ma and Graham 2000). Ambiguous results have been reported on the effect of EDTA on hydroxyl radical-generating systems (Li et al. 2007). Li et al. (2007) investigated the effect of EDTA on $\cdot OH$ production during Fenton reaction, and the result showed that EDTA did not affect $\cdot OH$ generation monitored by HPLC assay, but from the electron spin resonance (ESR) spin-trapping measurement, it was showed that EDTA suppresses hydroxyl radical formation. Kishimoto et al. reported that iron-chelating agents, such as EDTA, strongly inhibited (70%) the Fenton reaction at pH 2.5 or higher by complex formation with Fe(II) ion and masking of iron (Kishimoto et al. 2013). Similar inconsistent results were observed by Wang et al. (2011), who observed correlated well with the accelerated $\cdot OH$ formation from the H_2O_2 decomposition at the BiFeO₃ surface. Moreover, in the presence of phosphate, removal efficiency is reduced by 70%. Since phosphate and TBA are well-known $\cdot OH$ scavengers, the reduction of MG degradation in the presence of phosphate clearly confirms the generation of $\cdot OH$ in the EFP (Jafari et al. 2016). As deduced above, in the comparison with BQ, TBA had more inhibition impact on MG degradation. The degradation of MG was inhibited slightly with BQ, compared with the addition of TBA. Therefore, the effect of hydroxyl radical ($\cdot OH$) on MG degradation is greater than that of superoxide radical scavenger (O_2^-).

Conclusion

The performance of electro-Fenton process (EFP) was examined in the removal of MG from a concentrated aqueous solution. Several operational variables were studied for their effects on process efficacy. Narrow optimum pH (3) for the EFP limits the perfect application of this technology in wastewater treatment. The optimum ratio of H_2O_2 to Fe^{2+}

was determined to be approximately 0.11 (mg H_2O_2 to mg Fe^{2+}). It can be concluded that the EFP could completely degrade around 1000 mg/L MG at a short reaction time of 30 min under optimum condition. Reaction rate constants for EFP and ECP were acquired 0.092 and 0.02 min⁻¹, respectively. The results showed that TOC was reduced by 62.3% for 5 min and 95.3% for 30 min. It was found that the most important intermediates included aromatic compounds and benzoic acid. Results showed, in the comparison with BQ, TBA had more inhibition impact on MG degradation. Therefore, the oxidation by hydroxyl radicals is dominant mechanism of MG degradation. It can be concluded that the EFP can be an efficient process for the removal of MG wastewater containing such contaminants.

Acknowledgment We appreciate the Urmia University of Medical Science for providing financial and instrumental support to conduct this work.

Conflict of interest The authors have replied that they have no conflicts of interest to declare.

Open Access This article is licensed under a Creative Commons Attribution 4.0 International License, which permits use, sharing, adaptation, distribution and reproduction in any medium or format, as long as you give appropriate credit to the original author(s) and the source, provide a link to the Creative Commons licence, and indicate if changes were made. The images or other third party material in this article are included in the article's Creative Commons licence, unless indicated otherwise in a credit line to the material. If material is not included in the article's Creative Commons licence and your intended use is not permitted by statutory regulation or exceeds the permitted use, you will need to obtain permission directly from the copyright holder. To view a copy of this licence, visit <http://creativecommons.org/licenses/by/4.0/>.

References

- APHA (1998) American Public Health Association. Standard methods for the examination of water and wastewater, Water Environment Federation
- Arslan-Alaton I, Kobya M, Akyol A, Bayramoglu M (2009) Electrocoagulation of azo dye production wastewater with iron electrodes: process evaluation by multi-response central composite design. *Color Technol* 125(4):234–241
- Babuponnusami A, Muthukumar K (2012) Advanced oxidation of phenol: a comparison between Fenton, electro-Fenton, sono-electro-Fenton and photo-electro-Fenton processes. *Chem Eng J* 183:1–9
- Canizares P, Garcia-Gomez J, Saez C, Rodrigo MA (2004) Electrochemical oxidation of several chlorophenols on diamond electrodes: part II: influence of waste characteristics and operating conditions. *J Appl Electrochem* 34(1):87–94
- Cui D, Zhang H, He R, Zhao M (2016) The comparative study on the rapid decolorization of Azo, anthraquinone and triphenylmethane dyes by anaerobic sludge. *Int J Environ Res Public Health* 13(11):1053
- Culp SJ, Beland FA (1996) Malachite green: a toxicological review. *J American Coll Toxicol* 15(3):219–238
- Daneshvar N, Oladegaragoze A, Djafarzadeh N (2006) Decolorization of basic dye solutions by electrocoagulation: an

- investigation of the effect of operational parameters. *J Hazard Mater* 129(1):116–122
- Daneshvar N, Aber S, Vatanpour V, Rasoulifard MH (2008) Electro-Fenton treatment of dye solution containing Orange II: influence of operational parameters. *J Electroanal Chem* 615(2):165–174
- Dia O, Drogui P, Buelna G, Dubé R, Ihsen BS (2017) Electrocoagulation of bio-filtrated landfill leachate: fractionation of organic matter and influence of anode materials. *Chemosphere* 168:1136–1141
- Eiroa M, Kennes C, Veiga MC (2005) Simultaneous nitrification and formaldehyde biodegradation in an activated sludge unit. *Biore-sour Technol* 96(17):1914–1918
- El-Desoky HS, Ghoneim MM, Zidan NM (2010) Decolorization and degradation of Ponceau S azo-dye in aqueous solutions by the electrochemical advanced Fenton oxidation. *Desalination* 264(1):143–150
- Epa (2002) Environmental Protection Act. Standards for effluent discharge regulations. General Notice No. 44. of 2003. <http://faole.x.fao.org/docs/texts/mat52519.docS>. Accessed 09 March 11
- Forgiarini E, De Souza AAU (2007) Toxicity of textile dyes and their degradation by the enzyme horseradish peroxidase (HRP). *J Hazard Mater* 147(3):1073–1078
- Garcia-Segura S, Ocon JD, Chong MN (2018) Electrochemical oxidation remediation of real wastewater effluents—a review. *Process Saf Environ Prot* 113:48–67
- Ghaly AE, Ananthashankar R, Alhattab M, Ramakrishnan VV (2014) Production, characterization and treatment of textile effluents: a critical review. *J Chem Eng Process Technol* 5(1):1–18
- Ghoneim MM, El-Desoky HS, Zidan NM (2011) Electro-Fenton oxidation of Sunset Yellow FCF azo-dye in aqueous solutions. *Desalin Water Treat* 274(1–3):22–30
- Giannakis S, Hendaoui I, Jovic M, Grandjean D, De Alencastro LF, Girault H, Pulgarin C (2017) Solar photo-Fenton and UV/H₂O₂ processes against the antidepressant Venlafaxine in urban wastewaters and human urine. Intermediates formation and biodegradability assessment. *Chem Eng J* 308:492–504
- Gokulakrishnan S, Parakh P, Prakash H (2012) Degradation of Malachite green by Potassium persulphate, its enhancement by 1, 8-dimethyl-1, 3, 6, 8, 10, 13-hexaazacyclotetradecane nickel (II) perchlorate complex, and removal of antibacterial activity. *J Hazard Mater* 213:19–27
- Guenfoud F, Mokhtari M, Akrouit H (2014) Electrochemical degradation of malachite green with BDD electrodes: effect of electrochemical parameters. *Diamond Relat Mater* 46:8–14
- Guinea E, Garrido JA, Rodríguez RM, Cabot P-L, Arias C, Centellas F, Brillas E (2010) Degradation of the fluoroquinolone enrofloxacin by electrochemical advanced oxidation processes based on hydrogen peroxide electrogeneration. *Electrochim Acta* 55(6):2101–2115
- Hafaiedh NB, Bellakhal N (2015) Mineralization of synthetic and industrial food effluent containing acid Red18 by electro-Fenton process using a Graphite-Felt Cathode. *Int J Sci Res (IJSR)* 4(5):2643–2649
- Hameed BH, Lee TW (2009) Degradation of malachite green in aqueous solution by Fenton process. *J Hazard Mater* 164(2):468–472
- Hashemian S (2013) Fenton-like oxidation of Malachite green solutions: kinetic and thermodynamic study. *J Chem* 2013:7
- Hoffmann MR, Martin ST, Choi W, Bahnemann DW (1995) Environmental applications of semiconductor photocatalysis. *Chem Rev* 95(1):69–96
- Jafari SJ, Moussavi G, Hossaini H (2016) Degradation and mineralization of diazinon pesticide in UVC and UVC/TiO₂ process. *Desalin Water Treat* 57(8):3782–3790
- Jiang C-C, Zhang J-F (2007) Progress and prospect in electro-Fenton process for wastewater treatment. *J Zhejiang Univ* 8(7):1118–1125
- Khataee AR, Vatanpour V, Ghadim ARA (2009) Decolorization of CI Acid Blue 9 solution by UV/Nano-TiO₂, Fenton, Fenton-like, electro-Fenton and electrocoagulation processes: a comparative study. *J Hazard Mater* 161(2):1225–1233
- Kishimoto N, Kitamura T, Kato M, Otsu H (2013) Influence of chelating agents on Fenton-type reaction using ferrous ion and hypochlorous acid. *J Water Environ Technol* 11(1):21–32
- Li L, Abe Y, Kanagawa K, Shoji T, Mashino T, Mochizuki M, Tanaka M, Miyata N (2007) Iron-chelating agents never suppress Fenton reaction but participate in quenching spin-trapped radicals. *Anal Chim Acta* 599(2):315–319
- Li J, Luan Z, Yu L, Ji Z (2012a) Pretreatment of acrylic fiber manufacturing wastewater by the Fenton process. *Desalination* 284:62–65
- Li M-J, Li A-N, Xu X-R, Wu S, Li S, Ai X-X, Li H-B (2012b) Degradation and removal of malachite green in environment. *Int J Environ Bioenergy* 2(1):1–18
- Ma J, Graham NJD (2000) Degradation of atrazine by manganese-catalysed ozonation—influence of radical scavengers. *Water Res* 34(15):3822–3828
- Mitrowska K, Posyniak A, Zmudzki J (2008) Determination of malachite green and leucomalachite green residues in water using liquid chromatography with visible and fluorescence detection and confirmation by tandem mass spectrometry. *J Chromatogr A* 1207(1–2):94–100
- Moussavi G, Aghanejad M (2014) The performance of electrochemical peroxidation process for COD reduction and biodegradability improvement of the wastewater from a paper recycling plant. *Sep Purif Technol* 132:182–186
- Moussavi G, Khosravi R, Farzadkia M (2011) Removal of petroleum hydrocarbons from contaminated groundwater using an electrocoagulation process: batch and continuous experiments. *Desalination* 278(1–3):288–294
- Moussavi G, Bagheri A, Khavanin A (2012) The investigation of degradation and mineralization of high concentrations of formaldehyde in an electro-Fenton process combined with the biodegradation. *J Hazard Mater* 237–238:147–152
- Muruganandham M, Swaminathan M (2004) Decolourisation of Reactive Orange 4 by Fenton and photo-Fenton oxidation technology. *Dyes Pigm* 63(3):315–321
- Nidheesh PV, Gandhimathi R (2012) Trends in electro-Fenton process for water and wastewater treatment: an overview. *Desalination* 299:1–15
- Oturan MA, Guivarch E, Oturan N, Sirés I (2008) Oxidation pathways of malachite green by Fe³⁺-catalyzed electro-Fenton process. *Appl Catal B* 82(3):244–254
- Panizza M, Cerisola G (2009a) Direct and mediated anodic oxidation of organic pollutants. *Chem Rev* 109(12):6541–6569
- Panizza M, Cerisola G (2009b) Electro-Fenton degradation of synthetic dyes. *Water Res* 43(2):339–344
- Panizza M, Oturan MA (2011) Degradation of Alizarin Red by electro-Fenton process using a graphite-felt cathode. *Electrochim Acta* 56(20):7084–7087
- Peralta-Hernández JM, Meas-Vong Y, Rodríguez FJ, Chapman TW, Maldonado MI, Godínez LA (2006) In situ electrochemical and photo-electrochemical generation of the fenton reagent: a potentially important new water treatment technology. *Water Res* 40(9):1754–1762
- Pérez M, Torrades F, García-Hortal JA, Domènech X, Peral J (2002) Removal of organic contaminants in paper pulp treatment effluents under Fenton and photo-Fenton conditions. *Appl Catal B* 36(1):63–74
- Ray B, Lamsam A, Annachhatre A (2006) Treatment and management of wastewater from an acrylic fiber industry. In: International conference on sustainable development: issues and prospects for greater mekong subregion

- Rodrigo MA, Michaud PA, Duo I, Panizza M, Cerisola G, Comninellis C (2001) Oxidation of 4-chlorophenol at boron-doped diamond electrode for wastewater treatment. *J Electrochem Soc* 148(5):D60–D64
- Rodríguez M (2003) Fenton and UV-vis based advanced oxidation processes in wastewater treatment: degradation, mineralization and biodegradability enhancement. PhD Thesis, Universitat de Barcelona
- Santana-Casiano JM, Gonzalez-Davila M, Millero FJ (2006) The role of Fe(II) species on the oxidation of Fe(II) in natural waters in the presence of O₂ and H₂O₂. *Mar Chem* 99(1):70–82
- Shemer H, Linden KG (2006) Degradation and by-product formation of diazinon in water during UV and UV/H₂O₂ treatment. *J Hazard Mater* 136(3):553–559
- Sirés I, Brillas E, Oturan MA, Rodrigo MA, Panizza M (2014) Electrochemical advanced oxidation processes: today and tomorrow. *Rev Environ Sci Pollut Res* 21(14):8336–8367
- Srivastava S, Sinha R, Roy D (2004) Toxicological effects of malachite green. *Aquat Toxicol* 66(3):319–329
- Stolker AAM, Zuidema T, Nielen MWF (2007) Residue analysis of veterinary drugs and growth-promoting agents. *Trends Anal Chem* 26(10):967–979
- Szpyrkowicz L, Juzzolino C, Kaul SN (2001) A comparative study on oxidation of disperse dyes by electrochemical process, ozone, hypochlorite and Fenton reagent. *Water Res* 35(9):2129–2136
- Tchobanoglous G, Burton FL, Stensel HD (2003) *Wastewater engineering: treatment and reuse*. McGraw Hill, New York
- Ting W-P, Lu M-C, Huang Y-H (2008) The reactor design and comparison of Fenton, electro-Fenton and photoelectro-Fenton processes for mineralization of benzene sulfonic acid (BSA). *J Hazard Mater* 156(1):421–427
- Ting W-P, Lu M-C, Huang Y-H (2009) Kinetics of 2, 6-dimethylaniline degradation by electro-Fenton process. *J Hazard Mater* 161(2):1484–1490
- Wang C-T, Chou W-L, Chung M-H, Kuo Y-M (2010) COD removal from real dyeing wastewater by electro-Fenton technology using an activated carbon fiber cathode. *Desalination* 253(1):129–134
- Wang N, Zhu L, Lei M, She Y, Cao M, Tang H (2011) Ligand-induced drastic enhancement of catalytic activity of nano-BiFeO₃ for oxidative degradation of bisphenol A. *ACS Catal* 1(10):1193–1202
- Wanyonyi WC, Onyari JM, Shiundu PM, Mula FJ (2017) Biodegradation and detoxification of malachite green dye using novel enzymes from bacillus cereus strain KM201428: kinetic and metabolite analysis. *Energy Procedia* 119:38–51
- Xie Y, Wu K, Chen F, J He, J Zhao (2001) Investigation of the intermediates formed during the degradation of Malachite Green in the presence of Fe³⁺ and H₂O₂ under visible irradiation. *Res Chem Intermed* 27(3):237–248
- Xin X, Lang J, Wang T, Su Y, Zhao Y, Wang X (2016) Construction of novel ternary component photocatalyst Sr_{0.25}H_{1.5}Ta₂O₆·H₂O coupled with g-C₃N₄ and Ag toward efficient visible light photocatalytic activity for environmental remediation. *Appl Catal B* 181:197–209
- Zhou M, Yu Q, Lei L, Barton G (2007) Electro-Fenton method for the removal of methyl red in an efficient electrochemical system. *Sep Purif Technol* 57(2):380–387

Publisher's Note Springer Nature remains neutral with regard to jurisdictional claims in published maps and institutional affiliations.